SPARC enables genetic manipulation of precise proportions of cells

Jesse Isaacman-Beck [1], Kristine C. Paik[1,4], Carl F. R. Wienecke[1], Helen H. Yang[2], Yvette E. Fisher[2], Irving E. Wang[1,5], Itzel G. Ishida[3], Gaby Maimon[3], Rachel I. Wilson [2] and Thomas R. Clandinin [1✉]

Many experimental approaches rely on controlling gene expression in select subsets of cells within an individual animal. However, reproducibly targeting transgene expression to specific fractions of a genetically defined cell type is challenging. We developed Sparse Predictive Activity through Recombinase Competition (SPARC), a generalizable toolkit that can express any effector in precise proportions of post-mitotic cells in *Drosophila*. Using this approach, we demonstrate targeted expression of many effectors in several cell types and apply these tools to calcium imaging of individual neurons and optogenetic manipulation of sparse cell populations in vivo.

Genetic labeling and manipulation of small groups of cells has provided substantial insights into many aspects of biology and has been particularly impactful in studies of the nervous system. At one level, measurement and manipulation of molecularly defined cell types has become a common approach to neural circuit dissection[1]. In these approaches, cell-type-specific expression of transcription factors such as Gal4 (ref. [2]), recombinases such as Flp[3] and Cre[4], effector proteins such as green fluorescent protein (GFP)[5], reporters of neuronal activity such as GCaMP[6] and optogenetic tools such as channelrhodopsin[7] enables a wide range of measurements and perturbations. Especially powerful are paradigms in which one measures the phenotypes of stochastically selected subsets of cells of the same type, because these paradigms allow assays such as single-cell characterization and within-animal comparisons between manipulated and unmanipulated cells. As a result, genetic methods to achieve such sparse manipulations are of broad interest.

Several existing techniques can target fractions of cells of the same genetically defined cell type. In rodents, sequential recombinase-mediated switches[8,9], tamoxifen-induced Cre[10], Brainbow[11] or Mosaic Analysis with Double Markers (MADM)[12] can all label subpopulations of neurons. Similarly in *Drosophila*, Mosaic Analysis with a Repressible Cell Marker (MARCM[13]), Flybow and *Drosophila* Brainbow[14,15], chemically inducible destabilizing domains[16] and FlpOn or FlpOut approaches including MultiColor FlpOut (MCFO)[17–20] can be used to restrict effector expression. However, most of these techniques depend on limiting the spatial and/or temporal expression of a recombinase, and, in both mice and flies, they require time-consuming titration of chemical or gene induction conditions. Moreover, in flies, some of these techniques depend on Gal80 suppression of Gal4 (for example, FlpOut-Gal80 (ref. [17])) and cannot be used with some commonly used cell-type-selective drivers (split-Gal4 (ref. [21])). Other approaches (for example, MARCM) cannot be used in post-mitotic cells[13]. In addition, MCFO was paired with mutant recombinases with reduced activity to limit effector expression[20]. However, these recombinases might be expressed at different levels in different cell types, and, over time, as more recombinase is expressed, the fraction of labeled cells can change. Finally, whereas a wealth of refined Gal4 and split-Gal4 driver lines enable targeting of single cell types[22], selective manipulation of subsets of neurons within a driver line remains challenging. Thus, a toolkit with which one could a priori predict how many cells of a genetically identified type would be stochastically targeted would be of particular interest. Here we describe a technique to achieve this goal using a recombinase-dependent genetic competition with bistable outcomes whose balance can be precisely tuned by mutating recombinase target sites.

Results

Developing a strategy for building a bistable construct. In *Drosophila*, transgenes are often controlled by the heterologous Gal/UAS system in which the transcription factor Gal4 regulates expression of effector proteins via UAS sequences[2]. Building on this approach, we developed SPARC as a routine, all-genetic method for expressing effectors in defined fractions of post-mitotic cells of the same type. To do this, we generated a set of *UAS* constructs that can be switched on or off in different proportions of cells, depending on their sequences (Fig. 1 and Extended Data Fig. 1). We conditioned this switch on PhiC31 recombinase because it irreversibly recombines single *attP* and *attB* target sequences[23]. Furthermore, truncating canonical *attP* sequences diminishes the efficacy of recombination in *Escherichia coli*[24], creating the possibility of tunable genetic switches.

In an initial test of this idea, we designed two constructs in which PhiC31 enables Gal4-driven expression of the calcium indicator GCaMP6f by inverting the orientation of the coding sequence (Extended Data Fig. 1a,b). As a positive control, we flanked *GCaMP6f* with canonical *attP* and *attB* sequences, whereas, in our experimental construct, we truncated the *attP* to a 34-base pair (bp) sequence (*34bp_attP*) that mediates recombination in only 7% of reactions in *E. coli*[24]. We also generated transgenic flies that put expression of PhiC31 under the control of the neuronal synapto-brevin (nSyb) enhancer, a construct that should lead to high levels of recombinase expression in all post-mitotic neurons (*nSyb-PhiC31*; see Fig. 1, Extended Data Fig. 1 and Methods for more details).

[1]Department of Neurobiology, Stanford University, Stanford, CA, USA. [2]Department of Neurobiology and Howard Hughes Medical Institute, Harvard Medical School, Boston, MA, USA. [3]Laboratory of Integrative Brain Function and Howard Hughes Medical Institute, The Rockefeller University, New York, NY, USA. [4]Present address: Department of Medicine, Weill Cornell Medical College, New York, NY, USA. [5]Present address: Freenome, South San Francisco, CA, USA. ✉e-mail: trc@stanford.edu
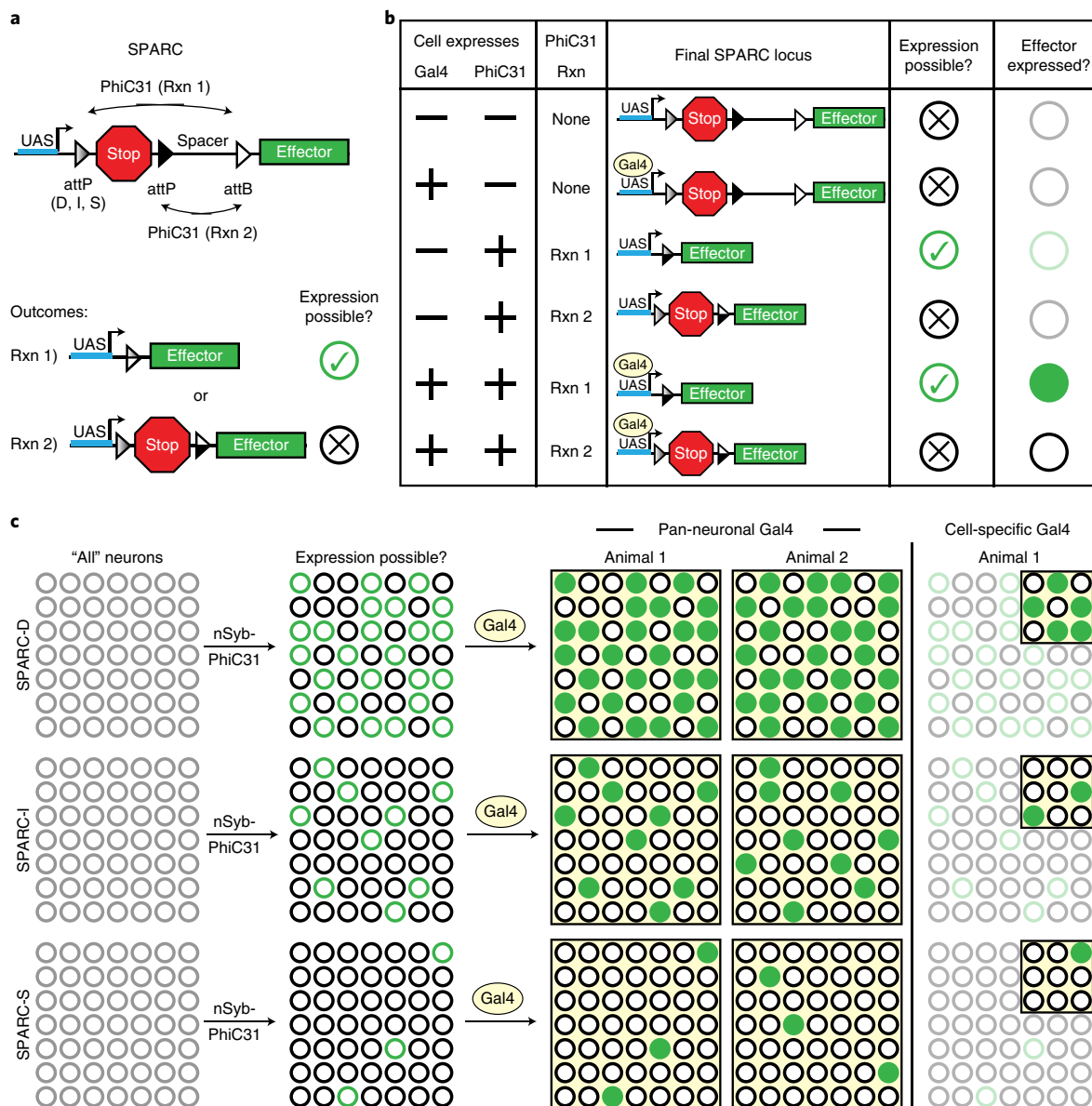
Fig. 1 | Schematic description of the SPARC method. a, Schematic of the SPARC cassette. PhiC31 recombines one of two competing *attP* target sequences with one *attB* target sequence. Progressively truncating the first *attP* favors retention of the stop cassette, preventing expression of effector (dense (D): 60 bp, canonical sequence; intermediate (I): 38 bp; sparse (S): 34 bp). Rxn 1 describes the cassette rearrangement that produces effector expression. Rxn 2 describes the cassette rearrangement that fails to produce effector expression. **b**, Table illustrating how PhiC31 and Gal4 expression in a cell can affect the SPARC cassette and SPARC effector expression. Effector expression occurs only in cells that express both PhiC31 and Gal4 and in which Rxn 1 occurs. **c**, Schematic of SPARC effector expression in cell populations. PhiC31 expressed from *nSyb-PhiC31* recombines the SPARC cassettes in all cells, rendering Gal4/UAS expression of the effector possible (Rxn 1; open green circle) or not possible (Rxn 2; open black circle) in three predictable proportions depending on the sequence of the first *attP* in the SPARC cassette (D, I or S). Gal4 is expressed in either all of these neurons (pan-neuronal Gal4) or a subset of these neurons (cell-specific Gal4) but can only drive effector expression (closed green circle) in the stochastic subset of cells in which SPARC Rxn 1 has occurred. Because the SPARC reaction is stochastic, different animals (animal 1, animal 2) will express effector in different subsets of cells within the Gal4 pattern.

To test these constructs, we used a well-defined Gal4 driver line that is active in Mi1 neurons (*Mi1-Gal4*), a population of 750 cells in each optic lobe. In *Mi1-Gal4* flies bearing *nSyb-PhiC31* and the control construct, we observed GCaMP6f expression in 100% of Mi1 cells by day 2 after eclosion (data not shown). Thus, PhiC31 can rapidly recombine *attP* and *attB* sequences in post-mitotic neurons. In contrast, using the *34bp_attP* construct, we observed GCaMP6f expression in sparse but variable fractions of neurons at day 2 after eclosion (Extended Data Fig. 1c–c"). However, by

day 6 after eclosion, nearly 100% of Mi1 neurons were labeled in flies bearing this *34bp_attP* construct (Extended Data Fig. 1d–d"). These results demonstrate that truncating the *attP* sequence reduces the efficiency of PhiC31 recombination in vivo, but, in the presence of PhiC31, recombination continues to occur until every neuron is labeled. Therefore, like other sparse labeling methods (for example, FlpOut), using these inversion constructs would require laborious titration of the recombinase to achieve reproducible sparse labeling.
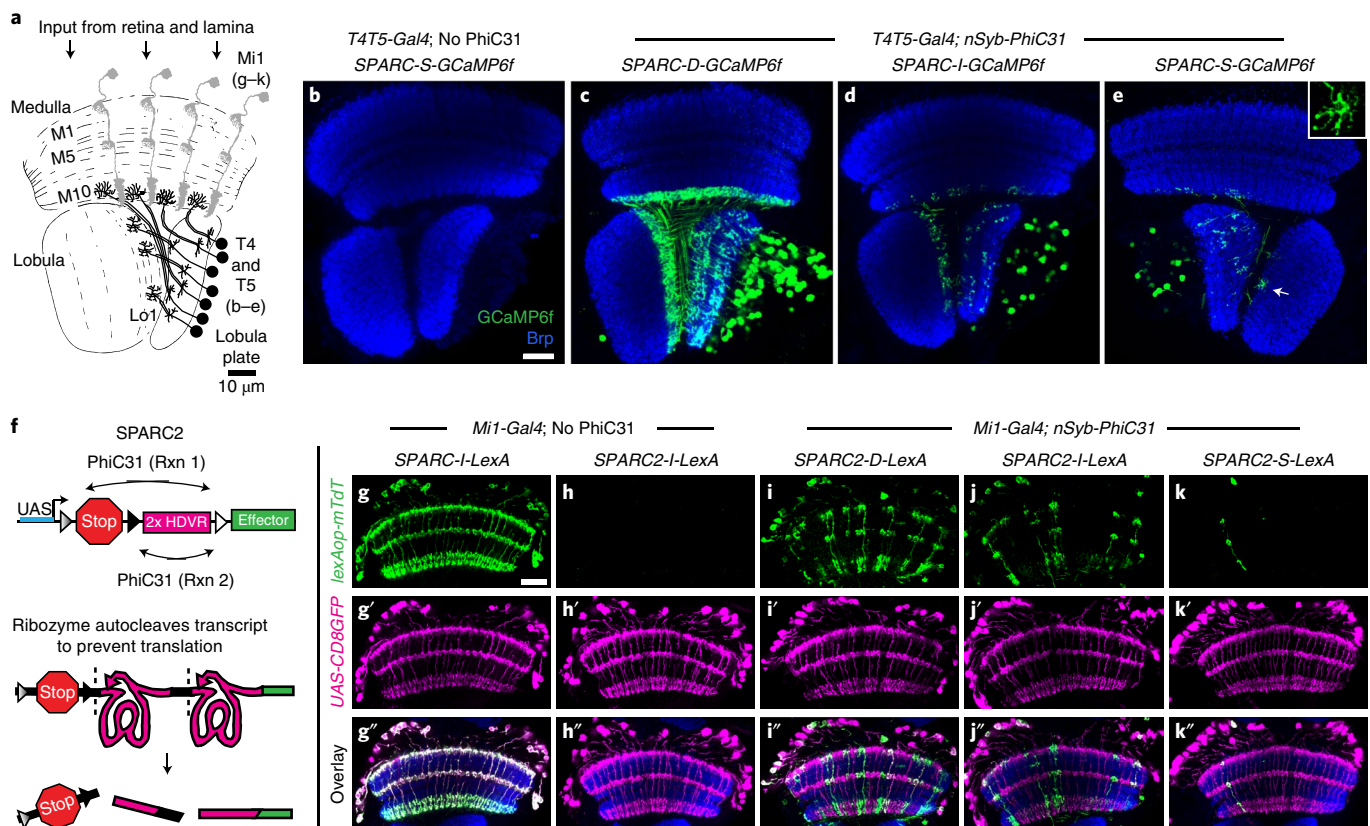
Fig. 2 | The SPARC toolkit enables predictable expression of effectors at three levels. a, Schematic of the *Drosophila* optic lobe highlighting T4, T5 and Mi1 (ref. [45]). **b–e**, GCaMP6f expression (green) in T4 and T5 neurons counterstained with anti-Bruchpilot (Brp, synaptic protein; blue). **b**, *SPARC-S-GCaMP6f*, no PhiC31. **c**, *SPARC-D-GCaMP6f*. **d**, *SPARC-I-GCaMP6f*. **e**, *SPARC-S-GCaMP6f*; arrow points to dendrite shown in inset. *n* > 10 optic lobes per genotype, observed in three independent experiments. **f**, Schematic of the SPARC2 cassette including the 2× hepatitis delta virus ribozyme (HDVR) sequence. **g–k**, LexA::p65-driven expression of myr::tdTomato (green, **g–k**), in Mi1 neurons (magenta, **g′–k′**) counterstained with anti-Bruchpilot (Brp; blue, overlay, **g″–k″**). **g**, *SPARC-I-LexA::p65*, no PhiC31. **h**, *SPARC2-I-LexA::p65*, no PhiC31. **i**, *SPARC2-D-LexA::p65*. **j**, *SPARC2-I-LexA::p65*.
k, *SPARC2-S-LexA::p65*. Scale bars, 10 μm. *n* > 10 optic lobes per condition, observed in three independent experiments.

We reasoned that one way to make expression of the effector a discrete outcome would be to force PhiC31 to choose between two alternative recombination events. To do this, we designed a bistable *UAS* construct that could lead to expression of one of two effectors, Flp or LexA (Extended Data Fig. 1e). Here, we set up a competition wherein PhiC31 could recombine either of two canonical *attP* sequences with a single *attB* sequence. As a result, PhiC31 will either flip the LexA coding sequence into the correct orientation for Gal4-driven expression (reaction 1 (Rxn 1)) or excise the intervening sequence, allowing for Flp recombinase expression (reaction 2 (Rxn 2)). Using this construct, the outcome is discrete and irreversible because both reactions destroy the *attB* sequence. We generated flies harboring this bistable construct, *nSyb-PhiC31*, fluorescent reporters for LexA (*lexAop-myr::tdTomato*) and Flp (*UAS-FRT-stop-FRT-mCD8::GFP*[25]) and *Mi1-Gal4*. In these flies, we observed that either Rxn 1 or Rxn 2 happened in every Mi1 neuron by day 3 after eclosion (Extended Data Fig. 1f–f″). Analogous results were observed using a pan-neuronal Gal4 (*nSyb-Gal4* (ref. [26]); data not shown). As these reactions went to completion, we infer that our *nSyb-PhiC31* construct expressed sufficiently high levels of recombinase to act on the bistable switch in each neuron. However, we were surprised to note that Rxn 1 and Rxn 2 occurred at different relative frequencies even though two identical *attP* sequences were involved. In this construct, Rxn 1 and Rxn 2 are topologically distinct, as one produces an inversion and the other an excision. We therefore sought a tunable cassette in which two reactions with identical topologies could result in discrete outcomes.

Tuning sparse labeling to achieve different levels of targeting.
Building on these principles, we designed SPARC, a second generation of bistable *UAS* constructs. In these constructs, two excision reactions can occur, one of which leads to effector expression and one of which does not (Fig. 1a,b). In Rxn 1, recombination between the first *attP* sequence and the *attB* removes a stop cassette to enable effector expression in cells expressing Gal4 (Fig. 1a,b). The reaction using the second *attP* leaves this stop sequence intact and prevents expression (Rxn 2; Fig. 1a,b). Based on our inversion constructs (Extended Data Fig. 1a,b), we reasoned that progressively truncating the first *attP* relative to the second *attP* would shift the equilibrium between Rxn 1 and Rxn 2 to favor retention of the stop cassette. This would tune the sparseness of effector expression by limiting expression to a smaller fraction of a cell population (Fig. 1c). Based on their recombination efficiencies in *E. coli*, we generated constructs with three different *attP* variants[24] in the first position (canonical: 60bp_*attP*, truncated: 38bp_*attp* or 34bp_*attp*; Extended Data Fig. 2, and see Methods for full sequences) that we predicted would target different fractions of cells (D-Dense, I-Intermediate and S-Sparse, respectively). Taking these together, SPARC works as follows. PhiC31 expressed from *nSyb-PhiC31* rapidly recombines the SPARC construct in all neurons, and the proportion of neurons in which Rxn1 has occurred that can express effector is dictated by the *attP* variant (D, I or S; Fig. 1c). The Gal4 expression pattern determines the selected cell type, and Gal4 successfully drives effector expression in the subset of these cells in which Rxn 1 occurred. Finally, as the recombinase reaction is stochastic and independent
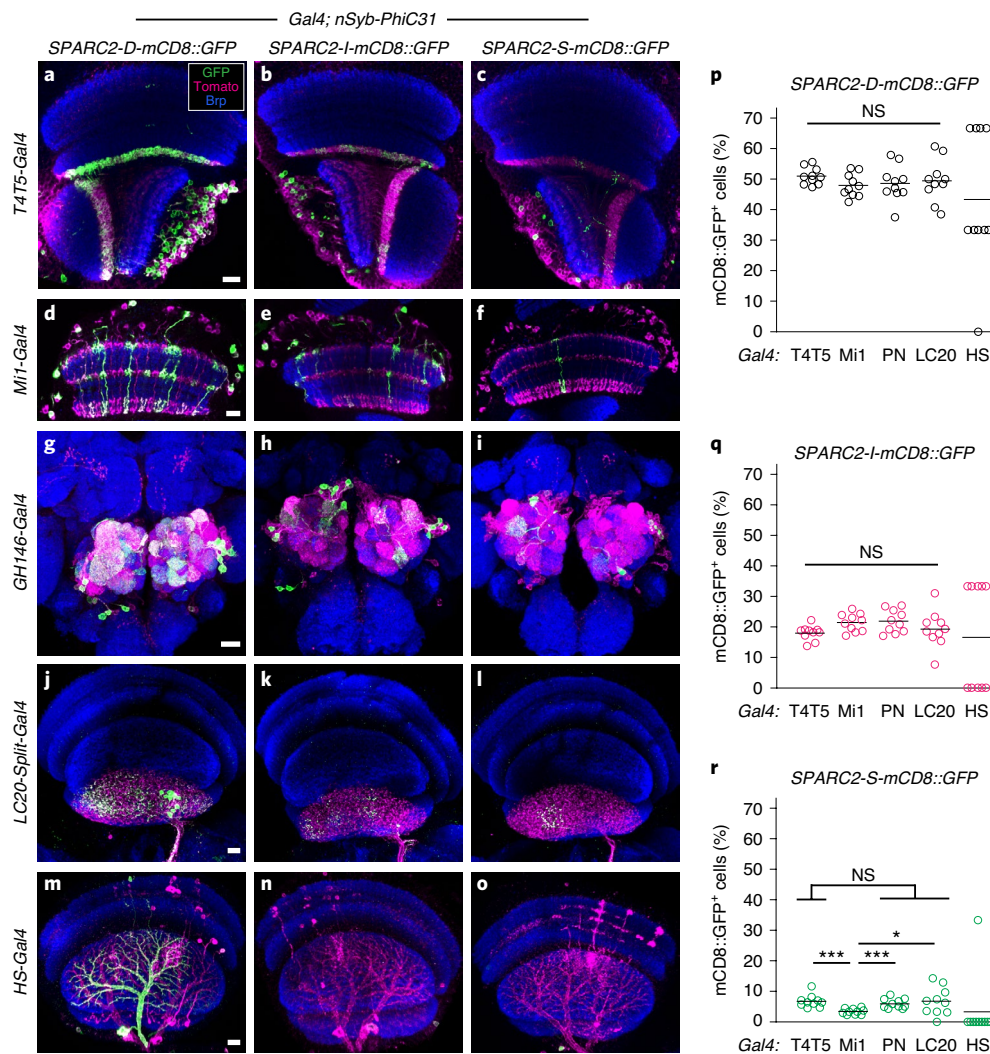
Fig. 3 | SPARC2 labels precise proportions of neurons across a diverse set of cell types. a–o, *SPARC2-mCD8::GFP* expression (green) in different neuron populations (magenta) counterstained with anti-Bruchpilot (Brp; blue). *SPARC2-D-mCD8::GFP*, *SPARC2-I-mCD8::GFP* and *SPARC2-S-mCD8::GFP* in the following cell types: (**a–c**) T4 and T5 neurons, (**d–f**) Mi1 neurons, (**g–i**) olfactory PNs in the *GH146-Gal4*^{+} population, (**j–l**) LC20 neurons and (**m–o**) HS neurons. **p–r**, Percentage of neurons labeled by different SPARC2 modules. **p**, *SPARC2-D-mCD8::GFP* (black circles). **q**, *SPARC2-I-mCD8::GFP* (magenta circles). **r**, *SPARC2-S-mCD8::GFP* (green circles). *n* = 10 optic lobes or antenna lobes per genotype, from two independent experiments; bars indicate mean value. Scale bars, 10 μm (**a–i**) or 15 μm (**j–o**). NS, not significant (one-way ANOVA); *P = 0.03 (Mi1 versus LC20) and ***P = 0.0002 (Mi1 versus T4T5) or P = 0.0003 (Mi1 versus PN; two-sided Student's *t*-test). Within a cell type, all differences between D, I and S variants are statistically significant (P < 0.0001, two-sided Student's *t*-test). We excluded HS from statistical analyses (Methods).

in each neuron, the particular subset of cells that undergo Rxn 1 or Rxn 2 will vary between animals (Fig. 1c).

SPARC and SPARC2 enable effector expression at three levels. We first tested these constructs in one of the largest genetically defined populations of neurons in the *Drosophila* optic lobe, T4 and T5 cells[27] (Fig. 2a–e). In the absence of PhiC31, SPARC constructs retained the stop sequence, and T4T5-Gal4 failed to drive expression of *SPARC-GCaMP6f* (Figs. 1a, 2b; data not shown). When we paired the SPARC variants with *nSyb-PhiC31*, we observed progressively fewer GCaMP6f-labeled neurons from SPARC-D to SPARC-I to SPARC-S (Fig. 2c–e). *SPARC-D-GCaMP6f* labeled many overlapping neurons; *SPARC-I-GCaMP6f* labeled an intermediate number of neurons; and *SPARC-S-GCaMP6f* labeled individual neurons whose dendrites could be visualized (Fig. 2e, inset). We observed similar results in Kenyon cells, lobula columnar neurons and several columnar neurons in the optic lobe (Extended Data Fig. 3 and data not shown). These data are consistent with the notion that SPARC

variants can determine the fraction of cells that express effector across cell types and animals.

To generalize the SPARC technique, we next made *SPARC-LexA::p65* transgenes. LexA::p65 is a transcription factor that drives expression of transgenes under the control of the lexAop promoter[28]; this system is orthogonal to the Gal4/UAS expression system[29]. Using *SPARC-LexA::p65* in the absence of PhiC31 recombinase, 100% of neurons expressed LexA::p65, as assayed using *lexAop-myr::tdTomato*. (Fig. 2g–g"). This result suggested that the widely used stop cassette[28] that we used in the initial SPARC design (Fig. 1a) might permit a low level of read-through that can be detected by sensitive outputs like LexA::p65 (and mCD8::GFP; data not shown).

To avoid this read-through, we generated SPARC2, in which we incorporated two self-cleaving ribozymes from the hepatitis delta virus (HDV) into the SPARC module (Fig. 2f). We reasoned that these self-cleaving ribozymes should truncate any read-through transcript before translation[30,31]. We first examined
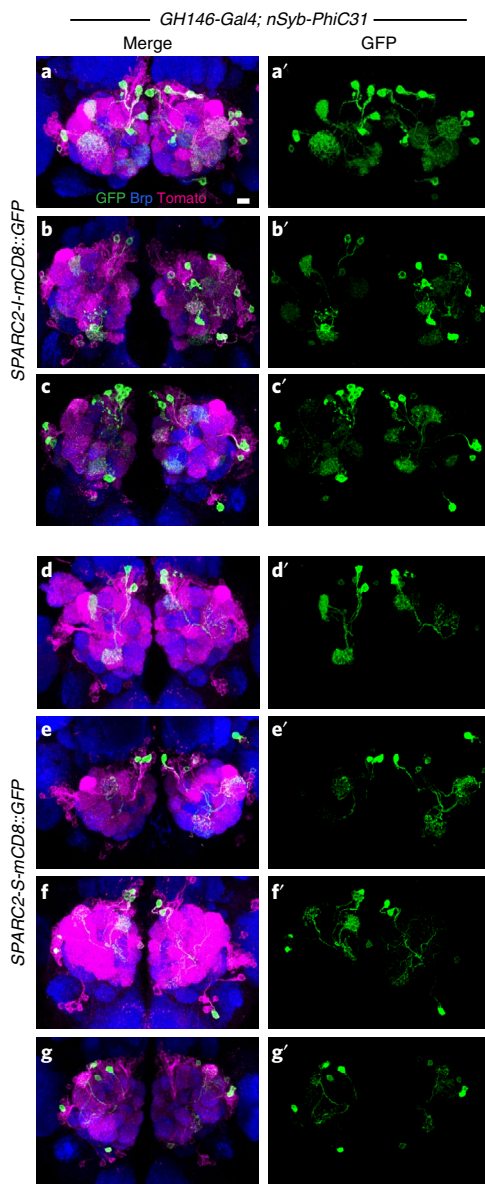
Fig. 4 | SPARC2 stochastically labels different subsets of neurons in each animal. a–g, SPARC2-mCD8::GFP expression (green) in olfactory PNs targeted by *GH146-Gal4* (magenta; myr::tdTomato reporter) counterstained with anti-Bruchpilot (Brp; blue). (**a–c'**) *SPARC2-I-mCD8::GFP* and (**d–g'**) *SPARC2-S-mCD8::GFP*. Seven brains are shown, representative of *n* = 10 brains per genotype. Scale bar, 10 μm.

SPARC2-LexA::p65 transgenes in Mi1 neurons in the absence of PhiC31 and observed a 10,000-fold decrease in read-through (~0.01% of Mi1 cells labeled with myr::tdTomato, Fig. 2h–h"; data not shown). Notably, in the presence of PhiC31, the D, I and S variants of *SPARC2-LexA::p65* behaved qualitatively similarly to the corresponding *SPARC-GCaMP6f* transgenes (Fig. 2i–k"). Thus, HDV ribozymes effectively eliminate read-through and enable SPARC2 transgenes to express both direct and amplifying effectors in three different proportions of cells.

Quantitative validation of SPARC2 efficacy across cell types. Our goal was to build a toolkit that could predictively target desired fractions of individual neurons within any population. In the *Drosophila* brain, identified neuronal populations vary widely in number. For example, in the visual system, there are approxi-

mately 6,000 T4 and T5 neurons per optic lobe[27] but only three HS neurons[32]. We first determined whether the three SPARC2 variants (D, I and S) allow targeting of different fractions of individual neurons across animals and cell types by generating *SPARC2-mCD8::GFP* transgenes and observing SPARC2 labeling at all three levels in five different neuronal populations: T4 and T5 (~6,000 cells per optic lobe[27], Fig. 3a–c), Mi1 (~750 cells per optic lobe[33], Fig. 3d–f), GH146+ olfactory projection neurons (PNs, ~91 cells per antenna lobe[34], Fig. 3g–i), LC20 (~29 cells per optic lobe[35], Fig. 3j–l) and HS (three neurons per optic lobe[32], Fig. 3m–o). To quantify how precise the SPARC2 variants are at targeting specific fractions of cells across different animals and distinct cell types, we co-labeled all Gal4-expressing cells with UAS-driven myr::tdTomato and quantified the mCD8::GFP-labeled neurons as a percentage of the total population (Fig. 3p–r). Remarkably, for each SPARC2 variant, mCD8::GFP was expressed in a similar percentage of neurons across cell types. *SPARC2-D-mCD8::GFP* labeled ~48–51% of cells, *SPARC2-I-mCD8::GFP* labeled ~17–22% of cells and *SPARC2-S-mCD8::GFP* labeled ~3–7% of cells (Fig. 3p–r).

A common experimental goal is to selectively label individual cells within a population. Impressively, despite cell numbers that span more than three orders of magnitude, we were able to reliably label individual cells in each population with at least one of the three SPARC2 variants. We labeled individual T4 and T5 dendrites with SPARC2-S (Fig. 3c). For Mi1, SPARC2-I labeled the most non-overlapping cells (Fig. 3e), although SPARC2-S also labeled individual neurons (Fig. 3f). SPARC2-I and SPARC2-S were similarly effective in labeling individual GH146+ olfactory PNs (Fig. 3h,i) or LC20 neurons (Fig. 3k,l), whereas both SPARC2-D and SPARC2-I routinely labeled individual HS neurons (Fig. 3m,n,p,q). As this set of cell types spans the full range of variation in neuron population size in the *Drosophila* brain, these data demonstrate that single-cell isolation can now be routine using the SPARC2 toolkit.

SPARC and SPARC2 effector expression are stochastic. To determine whether SPARC2 labeled stochastically distributed subsets of neurons across animals, we took advantage of the *GH146-Gal4* pattern that targets approximately 91 olfactory PNs in every animal[34] (Fig. 4a–g'). These PNs innervate distinct glomeruli in the antenna lobe, making it easy to determine whether distinct subsets of neurons are labeled in different animals. Consistent with the stochastic nature of PhiC31 recombination, we observed different patterns of PN labeling in every *SPARC2-I-mCD8::GFP* and *SPARC2-S-mCD8::GFP* animal (*n* = 10 each; Fig. 4 and data not shown). We observed similar results using other Gal4 drivers and SPARC and SPARC2 effectors (data not shown). In summary, these data demonstrate that the SPARC and SPARC2 toolkit reliably labels precise proportions of neurons that are stochastically distributed and can be revealed with any Gal4 driver.

SPARC and SPARC2 enable facile neural circuit measurement and perturbation. To investigate the functional utility of SPARC, we used SPARC-S-GCaMP6f to image calcium (Ca²⁺) responses in the dendrites of individual T5 neurons. These neurons preferentially respond to visual motion in one direction, a direction selectivity that is first observed in their dendrites[36,37]. As the dendrites of individual T5 neurons lie in close physical proximity and can have different direction selectivities, labeling individual cells is critical to measuring their functional properties. Previous attempts to image from individual T5 cells relied on laborious FlpOut approaches that required titrated and temporally precise heat shocks of *Drosophila* larvae to restrict effector expression to a subset of cells[37–39]. In contrast, the SPARC method consistently labeled fewer T5 neurons that were more distributed throughout the *T4T5-Gal4*+ population than the sparsest FlpOut labeling that we could achieve using a brief and
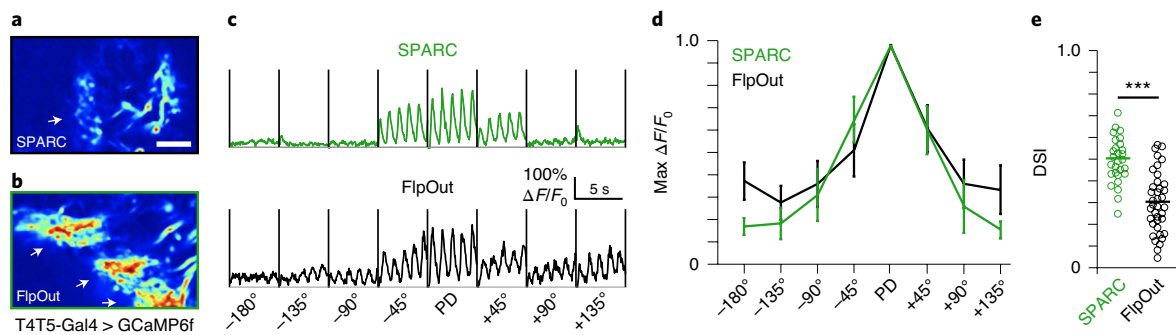
Fig. 5 | SPARC enables calcium imaging of single neurons. a,b, Normalized averaged fluorescence intensity of GCaMP6f in T5 dendrites sparsely labeled using (**a**) *SPARC-S-GCaMP6f* or (**b**) *FlpOut-Gal80*-enabled expression. Arrows point to dendrites. $n = 8$ experiments. **c,d,** GCaMP6f fluorescence responses ($\Delta F/F_0$) of T5 dendritic ROIs to sinusoidal gratings moving in one of eight different directions. PD denotes the preferred direction of each cell with the angular deviation from PD in degrees. **c,** Averaged responses of a representative ROI expressing GCaMP6f using *SPARC-S-GCaMP6f* (green) or *FlpOut-Gal80*-enabled expression (black). $n = 8$ experiments. **d,** Normalized tuning curves averaged across all T5 dendritic ROIs. $n = 8$ flies and 37 units per condition. Center values indicate means; error bars show one s.d. from the mean. **e,** DSI for each T5 dendritic ROI. $n = 8$ flies and 37 units per condition. ***$P = 3.75 \times 10^{-10}$ (two-tailed Student's *t*-test). Bars represent the mean. Scale bar, 10 μm.
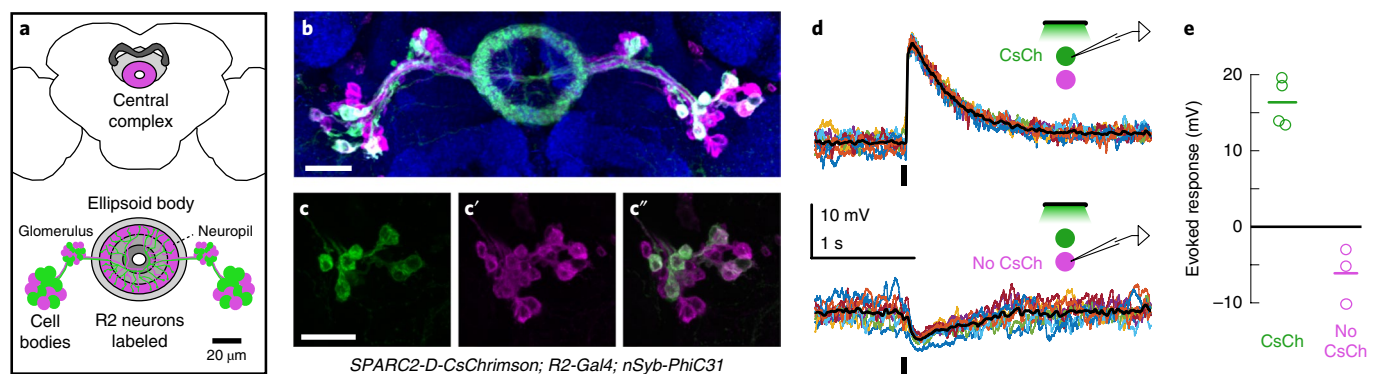

Fig. 6 | SPARC2 enables optogenetic stimulation of sparse cell populations. a, Schematic of the central complex and ellipsoid body depicting SPARC2-labeled R2 ring neurons. **b,** SPARC2-D-CsChrimson::tdTomato-3.1 expression (tdTomato; green) in R2 neurons (mCD8::GFP; magenta) counterstained with anti-Bruchpilot (Brp; blue). Image is representative of five individual brains stained from two independent experiments. **c–c″,** Closeup of cell bodies on the right in **b** showing (**c**) CsChrimson expression in (**c'**) R2 cells. **c″,** Overlay. **d,** Current-clamp recordings of single tdTomato⁺ (top) and tdTomato⁻ (bottom) R2 neurons. Stimulus is a 50-ms pulse of green light (vertical bar); ten trials each (colored lines); mean response (black line). **e,** Average evoked response (open circles) and mean population response (line) of R2 neurons, both tdTomato⁺ (green, $n = 4$) and tdTomato⁻ (magenta, $n = 3$). Each neural recording (**d,e**) was an independent experiment. Scale bars, 20 μm.

developmentally late heat shock (Fig. 5a,b). More importantly, when we imaged visually evoked Ca²⁺ responses in regions of interest (ROIs) representing T5 dendrites, we observed that the fluorescent signals from SPARC-labeled ROIs were significantly more direction selective than those from FlpOut-labeled ROIs (direction selectivity index (DSI); Fig. 5c–e). This result reflects the fact that SPARC labeling was sparser than the sparsest FlpOut labeling that we could achieve. As a consequence, SPARC ROIs more cleanly captured signals from single cells, whereas FlpOut ROIs likely included signals from multiple labeled cells with different directional preferences (Methods). Thus, both anatomical and functional evidence suggests that SPARC isolates single T5 dendrites more easily and more consistently than standard FlpOut approaches.

To determine if we could use this approach to manipulate the activity of neuronal subpopulations, we generated *SPARC2-CsChrimson::tdTomato* transgenic flies[40]. We expressed this construct in ring (R) neurons—GABAergic neurons that send sensory input to the central complex[41]. R neurons are divided into types based on morphology[42]; here we focused on the R2 type. We expressed SPARC2-D-CsChrimson::tdTomato in a subset of R2

neurons (Fig. 6a–c") and performed whole-cell recordings from tdTomato⁺ and tdTomato⁻ R2 neurons. We observed that tdTomato⁺ R2 neurons were depolarized by light, whereas tdTomato⁻ R2 neurons were not depolarized (Fig. 6d,e). Indeed, tdTomato⁻ R2 neurons were slightly hyperpolarized by light, implying that these R2 neurons were inhibited by other R2 neurons that express CsChrimson. Thus, *SPARC2-CsChrimson* allows optogenetic activation of sparse cell populations within a single cell type, enabling the discovery of interactions among them, such as mutual inhibition.

Discussion

The existing SPARC and SPARC2 toolkit. The SPARC and SPARC2 toolkit provides facile manipulation of three precise proportions of any cell type. We include direct effector transgenes that can be used to label cells (mCD8::GFP), to observe changes in intracellular calcium concentration (GCaMP6f and jGCaMP7f) and membrane potential (ASAP2f), as well as to optogenetically modulate neuronal activity (CsChrimson). In addition, the availability of the indirect effector transgene *SPARC2-LexA::p65* opens the possibility of sparsely expressing a large range of additional existing effectors

under the control of *lexAop* (Extended Data Fig. 4). To provide the flexibility to target both neuronal and non-neuronal cells, we also generated transgenic animals that express PhiC31 pan-neuronally (*nSyb-PhiC31*), ubiquitously (*tub-PhiC31*) and in any cell type expressing Gal4 (*UAS-PhiC31*). As a result, we think that this toolkit will be broadly applicable in its current form.

Comparisons with other methods. Extant approaches to label precise proportions of cells required user titration of recombinase expression levels or activity. For SPARC and SPARC2, we bypass this effort through a construct that is designed to use a strong, saturating source of PhiC31 recombinase. To perform a diverse array of experiments on single cells or on precise proportions of cells of a given genetically defined type, one can simply generate flies with the appropriate combination of transgenes (Figs. 1–4; see Methods and Extended Data Fig. 4 for example crosses and restrictions on stock maintenance). Alternatively, if additional tuning of recombinase levels is required, one can use other PhiC31 sources, including the *UAS-PhiC31* transgene that we provide. Furthermore, unlike previous methods of sparse manipulation that depend on cell division (MARCM and MADM), SPARC and SPARC2 can circumvent development to specifically manipulate post-mitotic neurons. Finally, SPARC and SPARC2 can be easily paired with split-Gal4 drivers to label and manipulate very precisely defined cell populations.

Future modification and potential use cases of SPARC2. To ensure that any user can easily incorporate any current or future genetically encoded effector into this toolkit, we designed each element to be modular and easily manipulated (Extended Data Fig. 2 and Methods). For example, if one wanted to target other precise proportions of cells, one could explore further mutagenesis of SPARC2's *attP* or *attB* target sites[24], or one could exchange the position of the truncated *attP* and canonical *attP* within the SPARC2 cassette (that should enable effector expression in >50% of cells). Moreover, in addition to *nSyb-PhiC31*, the toolkit includes *UAS-PhiC31* and *tub-PhiC31* constructs and transgenic animals to alter where and when PhiC31 is expressed. In the context of the nervous system, SPARC, SPARC2 and future variations will allow convenient and unparalleled access to define single-neuron contributions to neural circuit processing. By making single-cell measurements and perturbations routine, we enable precise characterization of single-neuron properties. In non-neuronal cells, SPARC will enable wide-ranging studies that exploit mosaic analysis to investigate cell biology and physiology. Finally, as PhiC31 functions in both the mouse and fish[43,44], we anticipate that this strategy will be widely generalizable to other model systems.

Online content

Any methods, additional references, Nature Research reporting summaries, source data, extended data, supplementary information, acknowledgements, peer review information; details of author contributions and competing interests; and statements of data and code availability are available at https://doi.org/10.1038/s41593-020-0668-9.

References

1. Luo, L., Callaway, E. M. & Svoboda, K. Genetic dissection of neural circuits: a decade of progress. *Neuron* **98**, 256–281 (2018).
2. Duffy, J. B. GAL4 system in *Drosophila*: a fly geneticist's Swiss army knife. *Genesis* **34**, 1–15 (2002).
3. Golic, K. G. & Lindquist, S. The FLP recombinase of yeast catalyzes site-specific recombination in the *Drosophila* genome. *Cell* **59**, 499–509 (1989).
4. Sauer, B. & Henderson, N. Site-specific DNA recombination in mammalian cells by the Cre recombinase of bacteriophage P1. *PNAS* **85**, 5166–5170 (1988).
5. Yeh, E., Gustafson, K. & Boulianne, G. L. Green fluorescent protein as a vital marker and reporter of gene expression in *Drosophila*. *PNAS* **92**, 7036–7040 (1995).
6. Akerboom, J. et al. Optimization of a GCaMP calcium indicator for neural activity imaging. *J. Neurosci.* **32**, 13819–13840 (2012).
7. Fenno, L., Yizhar, O. & Deisseroth, K. The development and application of optogenetics. *Annu. Rev. Neurosci.* **34**, 389–412 (2011).
8. Atasoy, D., Aponte, Y., Su, H. H. & Sternson, S. M. A FLEX switch targets channelrhodopsin-2 to multiple cell types for imaging and long-range circuit mapping. *J. Neurosci.* **28**, 7025–7030 (2008).
9. Lin, R. et al. Cell-type-specific and projection-specific brain-wide reconstruction of single neurons. *Nat. Methods* **15**, 1033–1036 (2018).
10. Feil, R. et al. Ligand-activated site-specific recombination in mice. *Proc. Natl Acad. Sci. USA* **93**, 10887–10890 (1996).
11. Livet, J. et al. Transgenic strategies for combinatorial expression of fluorescent proteins in the nervous system. *Nature* **450**, 56–62 (2007).
12. Zong, H., Espinosa, J. S., Su, H. H., Muzumdar, M. D. & Luo, L. Mosaic analysis with double markers in mice. *Cell* **121**, 479–492 (2005).
13. Lee, T. & Luo, L. Mosaic analysis with a repressible cell marker for studies of gene function in neuronal morphogenesis. *Neuron* **22**, 451–461 (1999).
14. Hadjieconomou, D. et al. Flybow: genetic multicolor cell labeling for neural circuit analysis in *Drosophila melanogaster*. *Nat. Methods* **8**, 260–266 (2011).
15. Hampel, S. et al. *Drosophila* Brainbow: a recombinase-based fluorescence labeling technique to subdivide neural expression patterns. *Nat. Methods* **8**, 253–259 (2011).
16. Sethi, S. & Wang, J. W. A versatile genetic tool for post-translational control of gene expression in *Drosophila melanogaster*. *eLife* **6**, e04577 (2017).
17. Gordon, M. D. & Scott, K. Motor control in a *Drosophila* taste circuit. *Neuron* **61**, 373–384 (2009).
18. Bohm, R. A. et al. A genetic mosaic approach for neural circuit mapping in *Drosophila*. *Proc. Natl Acad. Sci. USA* **107**, 16378–16383 (2010).
19. Philipsborn, von et al. Neuronal control of *Drosophila* courtship song. *Neuron* **69**, 509–522 (2011).
20. Nern, A., Pfeiffer, B. D. & Rubin, G. M. Optimized tools for multicolor stochastic labeling reveal diverse stereotyped cell arrangements in the fly visual system. *Proc. Natl Acad. Sci. USA* **112**, E2967–E2976 (2015).
21. Dionne, H., Hibbard, K. L., Cavallaro, A., Kao, J.-C. & Rubin, G. M. Genetic reagents for making split-GAL4 lines in *Drosophila*. *Genetics* **209**, 31–35 (2018).
22. Jenett, A. et al. A GAL4-driver line resource for *Drosophila* neurobiology. *Cell Rep.* **2**, 991–1001 (2012).
23. Thorpe, H. M. & Smith, M. C. In vitro site-specific integration of bacteriophage DNA catalyzed by a recombinase of the resolvase/invertase family. *Proc. Natl Acad. Sci. USA* **95**, 5505–5510 (1998).
24. Groth, A. C., Olivares, E. C., Thyagarajan, B. & Calos, M. P. A phage integrase directs efficient site-specific integration in human cells. *Proc. Natl Acad. Sci. USA* **97**, 5995–6000 (2000).
25. Hong, W. et al. Leucine-rich repeat transmembrane proteins instruct discrete dendrite targeting in an olfactory map. *Nat. Neurosci.* **12**, 1542–1550 (2009).
26. Riabinina, O. et al. Improved and expanded Q-system reagents for genetic manipulations. *Nat. Methods* **12**, 219–222 (2015).
27. Pinto-Teixeira, F. et al. Development of concurrent retinotopic maps in the fly motion detection circuit. *Cell* **173**, 485–498 (2018).
28. Pfeiffer, B. D. et al. Refinement of tools for targeted gene expression in *Drosophila*. *Genetics* **186**, 735–755 (2010).
29. Lai, S.-L. & Lee, T. Genetic mosaic with dual binary transcriptional systems in *Drosophila*. *Nat. Neurosci.* **9**, 703–709 (2006).
30. Perrotta, A. T. & Been, M. D. A pseudoknot-like structure required for efficient self-cleavage of hepatitis delta virus RNA. *Nature* **350**, 434–436 (1991).
31. Wernet, M. F., Klovstad, M. & Clandinin, T. R. A *Drosophila* toolkit for the visualization and quantification of viral replication launched from transgenic genomes. *PLoS ONE* **9**, e112092 (2014).
32. Schnell, B. et al. Processing of horizontal optic flow in three visual interneurons of the *Drosophila* brain. *J. Neurophysiol.* **103**, 1646–1657 (2010).
33. Sanes, J. R. & Zipursky, S. L. Design principles of insect and vertebrate visual systems. *Neuron* **66**, 15–36 (2010).
34. Jefferis, G. S., Marin, E. C., Stocker, R. F. & Luo, L. Target neuron prespecification in the olfactory map of *Drosophila*. *Nature* **414**, 204–208 (2001).
35. Wu, M. et al. Visual projection neurons in the *Drosophila* lobula link feature detection to distinct behavioral programs. *eLife* **5**, e21022 (2016).
36. Maisak, M. S. et al. A directional tuning map of *Drosophila* elementary motion detectors. *Nature* **500**, 212–216 (2013).
37. Fisher, Y. E., Silies, M. & Clandinin, T. R. Orientation selectivity sharpens motion detection in *Drosophila*. *Neuron* **88**, 390–402 (2015).
38. Leong, J. C. S., Esch, J. J., Poole, B., Ganguli, S. & Clandinin, T. R. Direction selectivity in *Drosophila* emerges from preferred-direction enhancement and null-direction suppression. *J. Neurosci.* **36**, 8078–8092 (2016).
39. Wienecke, C. F. R., Leong, J. C. S. & Clandinin, T. R. Linear summation underlies direction selectivity in *Drosophila*. *Neuron* **99**, 680–688 (2018).

40. Klapoetke, N. C. et al. Independent optical excitation of distinct neural populations. *Nat. Methods* **11**, 338–346 (2014).
41. Seelig, J. D. & Jayaraman, V. Feature detection and orientation tuning in the *Drosophila* central complex. *Nature* **503**, 262–266 (2013).
42. Omoto, J. J. et al. Neuronal constituents and putative interactions within the *Drosophila* ellipsoid body neuropil. *Front. Neural Circuits* **12**, 103 (2018).
43. Mosimann, C. et al. Site-directed zebrafish transgenesis into single landing sites with the phiC31 integrase system. *Dev. Dyn.* **242**, 949–963 (2013).
44. Olivares, E. C. et al. Site-specific genomic integration produces therapeutic Factor IX levels in mice. *Nat. Biotechnol.* **20**, 1124–1128 (2002).
45. Fischbach, P. K. F. & Dittrich, A. P. M. The optic lobe of *Drosophila melanogaster*. I. A Golgi analysis of wild-type structure. *Cell Tissue Res.* **258**, 441–475 (1989).

Methods

Generation of plasmids for transgenesis. All plasmids were generated with In-Fusion cloning (Takara Bio) using the primers described in Supplementary Table 1 or were generated through synthesis and molecular cloning by GenScript Biotech. Constructs were sequence verified by single primer extension (Sequetech). We submitted the constructs from Supplementary Table 2 to Addgene. All other constructs are available upon written request.

PhiC31 recombinase construct synthesis. We generated three constructs to express PhiC31 recombinase under the control of different promoters: 20XUAS, tubulin (Tub) and nSyb. These constructs were built in the backbone of pJFRC7 (Addgene no. 26220)[28]. To generate pJFRC-20XUAS-IVS-PhiC31, we PCR amplified a Kozak consensus sequence followed by the PhiC31 recombinase open reading frame and a nuclear localization sequence (NLS) from vector pBS130 (ref. [46]) and cloned it into the backbone via XhoI and XbaI sites. To generate pJFRC-αTub84B-IVS-PhiC31, we PCR amplified the tubulin 1 alpha (αTub84B) promoter from pIDT-attB-Tub_NLSGal4DBDlink-PBT[46] and replaced the 20XUAS promoter in pJFRC-20XUAS-IVS-PhiC31 by cloning into the HindIII and BglII sites. To generate pJFRC-nSyb-IVS-PhiC31, the nSyb promoter was PCR amplified from the pattB-synaptobrevin-4-QFBDMD-G4AD-hsp70 plasmid (Addgene no. 46112)[26] and cloned into the pJFRC-αTub84B-IVS-PhiC31 backbone via BglII sites flanking the αTub84B promoter. We submitted the pJFRC-nSyb-IVS-PhiC31 plasmid to Addgene (Supplementary Table 1).

Synthesis of SPARC development, SPARC and SPARC2 CRISPR donor plasmids. To generate the CRISPR donor backbone plasmid, pHD-3xP3-dsRed-ΔattP, we used site-directed mutagenesis (Quikchange, Stratagene XL; Agilent) to replace the *attP* sequence in the CRISPR donor vector pHD-AttP-3XP3-dsRed[47] with unique KpnI and MluI restriction enzyme sites using primer pair 1 (Supplementary Table 1). To target the *attP40* region of the genome, we PCR amplified a 1,040-bp left homology arm (2 L:5106650...5107689) and an 1,168-bp right homology arm (2 L:5108423...5109590) from genomic DNA from the IsoD1 *Drosophila* strain[48]. These left and right homology arms were first cloned into PCR2.1d-topo (Invitrogen) using primer pairs 2 and 4 (Supplementary Table 3) and were then subcloned into pHD-3XP3-dsRed-ΔattP using primer pair 3 via NotI and primer pair 5 via SapI, respectively. Primer pairs 3 and 5 added external flanking guide RNA (gRNA) target sites to enable Cas9-mediated linearization of the donor sequence in vivo (Extended Data Fig. 2 and Supplementary Table 2).

Next, several SPARC development, SPARC and SPARC2 cassettes were synthesized by GenScript Biotech and cloned into the unique KpnI site (Extended Data Fig. 2 and Supplementary Table 3). We then swapped effectors in these SPARC and SPARC2 donor plasmids via In-Fusion cloning with SalI restriction digest (Clontech) or using the CloneEZ method (GenScript Biotech). Each SPARC and SPARC2 construct contains two *attP* sequences and one *attB* sequence; we used sequences previously defined in ref. [24]. The first *attP* has a variable sequence depending on the SPARC or SPARC2 variant (D, I and S; Fig. 1a and Extended Data Fig. 1). Below we list these sequences and how they are used in each SPARC or SPARC2 variant:

60bp_attP Sequence (D variant): CGGGGAGTAGTGCCCCAACTGGGGTA-ACCTTTGAGTTCTCTCAGTTGGGGGCGTAGGGTCG

38bp_attP Sequence (I variant):
CCCCAACTGGGGTAACCTTTGAGTTCTCTCAGTTGGGG

34bp_attP Sequence (S variant):
CCAACTGGGGTAACCTTTGAGTTCTCTCAGTTGG

70bp_attB Sequence: CTCGAAGCCGCGGTGCGGGTGCCAGGGCGTGCCCTTGGAGTCTCCCCGGGCGCGTACTCCACCTCACCCATC

For detailed construct maps of SPARC and SPARC2 as well as recommended methods for modular swapping of the effector, see Extended Data Fig. 2.

gRNA-targeting vector logic and synthesis. We defined gRNA targets for insertion around the *attP40* region of the genome using the publicly available search tool flybase.org/crispr/ (ref. [49]). The sequence and genomic location of these target sites as well as the synthetic gRNA used for donor plasmid linearization are described in Supplementary Table 4. We validated that these near-attP40 gRNA targets were present and unmutated in our CRISPR target flies (*y sc v; +; P{Nos-Cas9}attP2*, TH00787; a gift from Norbert Perrimon) by PCR amplification and sequencing. Finally, we generated the construct pCFD5-attP40-gRNA using previously described methods (http://www.crisprflydesign.org/plasmids/) by PCR amplifying the three gRNA components and inserting them into the pCFD5: U6:3-t::gRNA backbone (a gift from Simon Bullock, Addgene no. 73914) via Bbs-I. Two of these gRNAs targeted neighboring genomic regions near the attP40 genomic locus in our CRISPR–homology-directed repair (HDR) target flies. We added a third gRNA component that targeted the synthetic gRNA sequence that flanks the donor insertion sequence in our pHD donor vectors (Extended Data Fig. 2). This synthetic gRNA has no predicted off-target recognition in the *Drosophila melanogaster* genome.

Generation of transgenic flies. All PhiC31-expressing transgenic flies were generated using site-specific insertion into the genome (BestGene). These transgenes carry the mini-*white* marker; their genomic locations are listed in Supplementary Table 5.

SPARC transgenic flies were generated by BestGene via standard construct injections (100–500 ng donor construct and 75–250 ng gRNA construct) and CRISPR–HDR. Transformants were identified by expression of the marker 3xP3-DsRed, which was later excised from the genome using Cre recombinase as previously described[47]. We maintained three or more independent isolates for each transgene and tested them for expression and function.

Genomic insertion site validation. To validate the inserted SPARC transgenes near the *attP40* locus, we PCR amplified genomic DNA with primer pairs in which one primer recognizes a genomic sequence outside of the homology arm and the other recognizes a sequence within the transgene. For every SPARC or SPARC2 transgenic fly, we ensured amplification of a PCR product from both the 5′ and 3′ sides of the transgene. The primer pairs and expected product sizes are in Supplementary Table 6. All transgenic insertions were validated by PCR with the exception of *TI{20XUAS-SPARC-D-Chrimson::tdTomato-3.1}CR-P40*. This transgene is missing ~300 bp of the left homology arm. However, we validated the function of this transgene in Fig. 6.

Complete fly stock list, fly genotypes and origin of transgenes. A list of all transgenic flies generated in this study can be found in Supplementary Table 5. Fly genotyes (by figure) and origin of transgenes are listed in Supplementary Information.

Fly husbandry. All flies were raised on molasses-based food at 25 °C with the exception of CsChrimson-expressing flies, which were raised on Nutri-Fly German Food (no. 66–115, Genesee Scientific) containing all-*trans*-retinal (0.6 mM). Conditions for specific experiments are described below.

Brain dissection, immunolabeling and confocal imaging. Brain dissection, immunolabeling and confocal imaging were performed in two different laboratories with slightly different protocols.

For Figs. 2–4 and Extended Data Figs. 1, 3 (Clandinin laboratory). Brain dissections were performed on 4–6-day-old adult female flies. Flies were ordered in a fly collar; the proboscis and antennae were removed for each fly; and flies were perfused with freshly made 2% paraformaldehyde in phosphate-buffered lysine for 50 min. We removed the fixative and washed the brains three times with ice-cold phosphate-buffered saline (PBS) and then proceeded to extract the brains with fine forceps. Brains were stored in ice cold PBS + 0.1% Triton-X (PBS-Tx) for up to 2 h and then were moved to a PBS-Tx + 10% normal goat serum (NGS) blocking solution for 30 min at room temperature. We incubated the brains in the following primary antibodies for 3 d at 4 °C: anti-GFP (chicken, 1:2,000, Abcam), anti-Bruchpilot (nc82, mouse, 1:30, Developmental Studies Hybridoma Bank) and anti-DsRed (rabbit, 1:700, Takara Bio). The anti-GFP antibody recognized both GFP and GCaMP6f. The anti-DsRed recognized myr::tdTomato. After primary incubation, brains were washed three times for 15 min in PBS-Tx and then subjected to secondary staining for 2 h at room temperature. All secondary antibodies were diluted 1:200 in PBS-Tx + NGS; these included anti-chicken Alexa 488 (Life Technologies), anti-rabbit-Cy3 (Life Technologies) and anti-mouse Alexa 633 (Life Technologies). Brains were then washed three times for 15 min in PBS-Tx, incubated for at least 1 h in 70% glycerol for tissue clearing and mounted individually on glass slides in Vectashield (H-1000, Vector Laboratories) for confocal imaging.

Brains were imaged on a Leica SP8 confocal microscope. Series of between 20 and 100 optical sections (1–5-μm spacing; total, 20–200 μm) were imaged using either a Leica HC PL APO ×20/0.70 CORR CS oil immersion lens (N.A. 1.3) or a Leica HC PL APO ×40/1.30 CS2 ×40 oil immersion lens (N.A. 1.42). Tiffs of single confocal planes or maximum intensity projections (MIPs) were made in Imaris 9.3 (Oxford Instruments). For Fig. 2 and Fig. 3a–f, MIPs were from three ×3-μm sections (9 μm) of tissue. For Fig. 3g–i and Fig. 4, MIPs were from ~15 ×2-μm sections (30 μm) of tissue. For Fig. 3j–o, MIPs were from 15–20 ×3-μm sections (45–60 μm) of tissue. For Extended Data Fig. 3a-d, MIPs of mushroom bodies were generated from 15–20 5-μm optical sections, whereas images of cell bodies (Kenyon cells, Extended Data Fig. 3e-h") were taken from single optical sections.

Image processing. Tiffs of single confocal planes or MIPs were generated in Imaris 9.3 (Oxford Instruments) and subsequently rotated and cropped to the same dimensions using Adobe Photoshop. Brightness levels were uniformly adjusted in Adobe Photoshop across images that were compared within a figure.

Cell counting (Fig. 3). For all T4 and T5 samples and SPARC2-D- and SPARC2-I-labeled Mi1 samples, cell bodies were imaged at ×40 using a series of 10–12 optical sections spaced 1 μm apart as described above. Subsequently, single planes from the top, middle and bottom of these stacks were isolated for each optic lobe (n = 10 per condition), and individual tiffs were generated for myr::tdTomato and mCD8::GFP stains from these planes. We randomly shuffled these images, and a blinded author manually counted the individual cell bodies in each channel

in Adobe Photoshop. For SPARC2-S-labeled Mi1 cells, GH146-Gal4⁺ olfactory PNs, LC20 neurons and HS neurons, optical sections were taken through the full extent of Gal4-labeled cells 1–3 µm apart. Single-color three-dimensional projections were generated in Imaris for all samples, and all myr::tdTomato⁺ or mCD8::GFP cell bodies were counted separately. We calculated the percent of SPARC-labeled cells as total number of SPARC-labeled cells/total number of cells labeled in the Gal4 pattern by myr::tdTomato. We first used one-way ANOVA to determine whether there were statistically significant differences between the proportion of mCD8::GFP-labeled cells for each SPARC2 variant by cell type and for each cell type by SPARC2 variant. When significant differences were detected, we used pairwise two-tailed Student's t-tests to define statistical differences within groups. We excluded HS from statistical analyses as there are only three cells in this population, and we would not expect a normal distribution when labeling ~50%, ~20% or ~5% of cells in such a small population.

For Fig. 6 (Wilson laboratory). For immunostaining brain dissections, newly eclosed female flies that were raised on 0.6 mM all-*trans*-retinal-containing Nutri-Fly German Food (no. 66–115, Genesee Scientific) were collected on CO₂. The brains were then dissected out of the head in chilled external saline[50]. Immunostaining was then performed as follows. Brains were (1) fixed in 4% paraformaldehyde (15714, Electron Microscopy Sciences) in PBS (46–013-CM, Thermo Fisher Scientific) for 15 min at room temperature; (2) washed three times for 15 min with PBS with 0.44% Triton X-100 (PBST; T-8787, Sigma-Aldrich); (3) incubated in a blocking solution of 5% NGS (G9023, Sigma-Aldrich) in PBST for 20 min; (4) incubated in a primary antibody solution containing mouse anti-Bruchpilot antibody (1:25, nc82, Developmental Studies Hybridoma Bank), chicken anti-GFP (1:1,000, ab13970, Abcam) and rabbit anti-dsRed (1:500, 632496, Takara Bio) diluted in the NGS blocking buffer for 48 h at room temperature on a rotating nutator; (5) washed three times for 15 min with PBST; (6) incubated in a secondary antibody solution containing Alexa 488-conjugated goat anti-chicken (1:250, A-11039, Thermo Fisher Scientific), Alexa 568-conjugated goat anti-rabbit (1:250, A-11011, Thermo Fisher Scientific) and Alexa 633-conjugated goat anti-mouse (1:250, A-21050, Thermo Fisher Scientific) in blocking solution for 24 h at room temperature on a rotating nutator; and (7) washed three times for 15 min with PBST.

Brains were mounted on slides in Vectashield (H-1000, Vector Laboratories) in the anterior–posterior orientation and then imaged using a Leica SPE confocal microscope. Series of between 30 and 100 optical sections (1.0-µm spacing) were imaged using either an Olympus UPLFLN ×40 oil immersion lens (N.A. 1.3) or an Olympus PLAPON ×60 oil immersion lens (N.A. 1.42). MIPs of the cell body images were made in Fiji[51], and MIPs of the full R2 neuron morphology were made in Imaris 9.3 (Oxford Instruments).

Fly preparation for two-photon imaging. For two-photon imaging of T5, we used the enhancer fragment VT025965 to drive expression of Gal4 in T5 with high specificity[52]. Sparse expression of GCaMP6f was achieved using either a FlpOut or a SPARC strategy. For the FlpOut strategy, we used the genotype +/y w, P{hsFLP}; P{20XUAS-IVS-GCaMP6f}attP40/ P{αtubP(FRT.stop)Gal80}2; P{VT025965-Gal4} attP2/+. We heat shocked at 37 °C for 90 s during the late third instar stage of development[37]. This heat shock protocol yielded the sparsest expression pattern for this T5 driver. Shorter or developmentally later heat shock resulted in either no GCaMP6f expression or no observable GCaMP6f signals. For the SPARC strategy, we used the genotype +; TI{20XUAS-SPARC-S-GCaMP6f}CR-P40 /P{nSyb-IVS-PhiC31}su(Hw)attP5; P{VT025965-Gal4}attP2/ +.

All flies were female and were imaged within 5–7 d of eclosion. Flies were immobilized by chilling on ice and affixed with a custom-built mount with UV-cured optical epoxy (NOA 63, Norland Products). The cuticle, fat bodies and trachea of the left hemisphere were removed under ice-cold, artificial hemolymph without calcium[50] to expose the brain for imaging from above. During imaging, standard, carbogen-gassed, room temperature artificial hemolymph[50] was perfused across the brain at 150 ml h⁻¹.

Imaging and delivery of visual stimuli. Imaging and delivery of visual stimuli followed Leong et al.[38]. Fluorescence was monitored in vivo using two-photon microscopy. We used a Leica SP 5 II equipped with the HCX APO L ×20/NA1.00 water dipping lens (Leica). GCaMP6f was excited at 920 nm, and the power was ~5–8 mW at the stage. Recordings lasted ~3.5 min. GCaMP6f fluorescence signals were acquired with a band-pass filter (525/50 m) at ~20 Hz (bidirectional scanning at 1.4 kHz, across a field of view of 128 pixels × 256 pixels, rows × columns). Pixels measured ~290 × ~290 nm. The stimulus screen subtended ~60° × 90° (azimuth × elevation) of the left visual field. Visual stimuli were delivered with a LightCrafter 4500 DLP (Texas Instruments) using a 100-Hz frame rate. The LightCrafter was configured to use only the blue LED, and then the stimulus was filtered with a 447/60 band-pass filter (Semrock, IDEX Health & Science) and an ND1 filter (Thorlabs). The mean radiance was ~0.04 W sr⁻¹ m⁻².

Identification and selection of ROIs. ROI selection involved two stages: (1) automated segmentation[53] of GCaMP6f responses to moving sinusoidal gratings to obtain an initial set of ROIs, each representing approximately individual cells

and (2) exclusion of ROIs from this initial set if they did not match the known calcium response properties of T5 (refs. [37,38]) or if their spatiotemporal receptive fields did not lie in the center of the stimulus screen, yielding a final set of ROIs that best represent individual T5 dendritic arbors. As T5 dendrites are fine and interdigitating, this ROI selection strategy could not always isolate dendritic arbors of individual T5 cells, particularly for FlpOut clones, because the sparsest possible FlpOut expression pattern that we could achieve was denser than the sparsest possible SPARC expression pattern. GCaMP6f responses to moving light and dark edges were used to confirm dark contrast selectivity (data not shown), and the timing of responses to moving dark edges was used to determine whether the cell's spatiotemporal receptive field was centered on the stimulus screen (data not shown). Two ROIs that did not meet these criteria were not further analyzed and were excluded.

Stimulus design and data analysis for T5 calcium imaging experiments. We presented sinusoidal gratings (1 Hz, 25° per cycle, 100% contrast) moving for 5 s in eight equally spaced directions. Each 5-s bout was preceded by a 3-s 'blank' (a gray screen of luminance matching the mean luminance of the gratings). We presented three complete cycles of all eight directions, in a random order, for a total recording duration of ~3.5 min.

GCaMP6f fluorescence responses were quantified as the average $\Delta F/F_0$ across pixels within each ROI, where F_0 was defined as the mean fluorescence within each ROI during the final five frames of the 'blank' preceding each bout. Responses were averaged across all three bouts to obtain the mean response to each direction of motion (plotted in Fig. 5c). Tuning curves (Fig. 5d) were derived from these mean responses, plotted as the maximum $\Delta F/F_0$ for each direction, normalized by the maximum $\Delta F/F_0$ across directions (the preferred direction (PD) response) and registered across ROIs to align the PD response before averaging across ROIs. For each ROI, the DSI (Fig. 5e) was calculated as the vector average of response amplitudes to the eight directions of motion, normalized by the sum of response amplitudes to all eight directions of motion.

Flies with zero ROIs meeting selection criteria (Methods) or with no visually responsive ROIs were excluded from further analysis (zero SPARC flies and two FlpOut flies). These exclusion criteria were predetermined.

Fly preparation and dissection for electrophysiology. Newly eclosed virgin female flies were collected on ice approximately 1–4 h before the experiment. All were raised on 0.6 mM all-*trans*-retinal-containing Nutri-Fly German Food (no. 66–115, Genesee Scientific), and fly vials were wrapped in foil to prevent photo-conversion of the all-*trans*-retinal. At the beginning of each dissection, the fly was cold anesthetized.

The preparation holder consisted of a flat titanium foil secured in an acrylic platform, with the foil oriented parallel to the horizontal body plane; the fly's head and body were gently pushed partway through a hole in the foil. The head was pitched backward so that the anterior surface was oriented dorsally in the holder. The fly was always secured in the holder with epoxy (Loctite AA 3972) cured using a brief (<1-s) pulse of UV light (LED-200, Electro-Lite). After the dorsal portion of the head was covered in saline, a large hole was cut in the head capsule, and the retina and trachea on one side of the brain were removed to expose the neurons of interest. To reduce brain movement, muscle 16 was severed, and the proboscis was removed. An aperture was made in the perineural sheath around the somata of interest by ripping gently with fine forceps.

The external solution contained (in mM) 103 NaCl, 3 KCl, 5 N-tris(hydroxymethyl) methyl-2-aminoethane-sulfonic acid, 8 trehalose, 10 glucose, 26 NaHCO₃, 1 NaH₂PO₄, 1.5 CaCl₂ and 4 MgCl₂, with osmolarity adjusted to 270–273 mOsm. External solution was bubbled with 95% O₂ and 5% CO₂ and reached a final pH of 7.3. External solution was continuously perfused over the brain during electrophysiology.

Whole-cell patch-clamp recordings. In vivo whole-cell patch-clamp recordings were performed as described previously[54]. Patch pipettes were made from borosilicate glass (1.5 mm O.D., 0.86 I.D., no. BF150–86–7.5HP, Sutter Instrument) using a Sutter Instrument P-97 puller. Pipette resistance ranged from 5 to 12 MΩ. The internal solution contained (in mM) 140 potassium aspartate, 10 4-(2-hy droxyethyl)−1-piperazineethanesulfonic acid, 4 MgATP, 0.5 Na₃GTP, 1 ethylene glycol tetra-acetic acid, 1 KCl and 13 biocytin hydrazide. The pH was 7.3, and the osmolarity was adjusted to ~268 mOsm. Recordings were performed at room temperature.

To obtain patch-clamp recordings under visual control, we used an Olympus BX51WI microscope with a ×40 water immersion objective (LUMPlan FI/ IR NA 0.8, Olympus). GFP- and tdTomato-expressing neurons were identified using an Hg-lamp source (U-LH100HG, Olympus) with an eGFP long-pass filter (U-N41012, Chroma) or a TRITC-Cy3 filter (Chroma).

To visualize the brain for recordings, far-red light was delivered from a fiber-coupled LED (740 nm, M740F2, Thorlabs) via a ferrule patch cable (200-µm core, Thorlabs) plugged into a fiber optic cannula (Ø1.25 mm SS ferrule 200-µm core, 0.22 NA, Thorlabs) glued to the recording platform, with the tip of the cannula ~1 cm behind the fly.

Recordings were obtained using an Axopatch 200B amplifier and a CV-203BU head stage (Molecular Devices). Voltage signals were low-pass filtered at 5 kHz before digitization and then acquired with a NiDAQ PCI-6251 (National Instruments) at 20 kHz. Liquid junction potential correction was performed post hoc by subtracting 13 mV from recorded voltages[55]. When a stable whole-cell recording was achieved, the initial resting membrane potential was measured. Consistent with what one might expect from expression of a cation channel, we observed differences in the resting membrane potential and input resistance between cells expressing CsChrimson and control cells (described in Supplementary Table 7). During optogenetic stimulation, a constant hyperpolarizing current was applied to bring the cell's membrane potential to between −50 mV and −60 mV.

For optogenetic stimulation, the Hg-lamp source (U-LH100HG) was used to deliver a 50-ms pulse of green light (530–550 nm, 2–4 mW, TRITC-Cy3 filter cube, Chroma) via the objective. A shutter (Uniblitz) controlled the pulse duration.

Electrophysiology data analysis and data inclusion. To measure CsChrimson-evoked responses, the mean of ten replicate stimulation trials was taken and filtered using a median filter with a 20-ms window to remove the effect of spiking activity. Evoked response amplitudes were the largest deviation from baseline that occurred within the 500 ms after the optogenetic stimulation. The 1 s before stimulation was used as the measurement of baseline membrane voltage.

Cells were analyzed only if the resting membrane voltage of the cell was less than −30mV immediately after break in. One of eight recordings was excluded based on this criterion.

Statistics. The following statistical tests were used in this study: 1) one-way ANOVA (Figs. 3p–r) and 2) two-tailed Student's *t*-test (Figs. 3r, 5e and Extended Data Fig. 2). No statistical methods were used to predetermine sample sizes, but our sample sizes are similar to those reported in previous publications[20,39,55]. Data distribution was assumed to be normal for all experiments except for quantification of HS cell labeling (Fig. 3p–r). These HS cell data were excluded from statistical comparisons as described above.

Randomization and blinding. Stimulus presentation was randomized for the experiments in Fig. 5. Otherwise, data collection was not randomized. Cell counting for Fig. 3 was done by a blinded observer, but, otherwise, data collection and analysis were not performed blinded to the conditions.

More detailed information on statistics, data exclusions, randomization and blinding and reagents can be found in the Life Sciences Reporting Summary associated with this paper.

Reporting Summary. Further information on research design is available in the Nature Research Reporting Summary linked to this article.

Data availability
The data that support the findings of this study are available from the corresponding author upon reasonable request. Source data are provided with this paper.

Code availability
All analysis was carried out using custom-written MATLAB code: https://github.com/wienecke/SPARC. Visual stimuli were programmed with the OpenGL 1.0 API in Visual C#. All code is available on Github and will be made available upon reasonable request from the corresponding author. Source data are provided with this paper.

References
46. Gohl, D. M. et al. A versatile in vivo system for directed dissection of gene expression patterns. *Nat. Methods* **8**, 231–237 (2011).
47. Gratz, S. J. et al. Highly specific and efficient CRISPR/Cas9-catalyzed homology-directed repair in *Drosophila. Genetics* **196**, 961–971 (2014).
48. Silies, M. et al. Modular use of peripheral input channels tunes motion-detecting circuitry. *Neuron* **79**, 111–127 (2013).
49. Housden, B. E. et al. Identification of potential drug targets for tuberous sclerosis complex by synthetic screens combining CRISPR-based knockouts with RNAi. *Sci. Signal* **8**, rs9–rs9 (2015).
50. Wilson, R. I., Turner, G. C. & Laurent, G. Transformation of olfactory representations in the *Drosophila* antennal lobe. *Science* **303**, 366–370 (2004).
51. Schindelin, J. et al. Fiji: an open-source platform for biological-image analysis. *Nat. Methods* **9**, 676–682 (2012).
52. Leonhardt, A. et al. Asymmetry of *Drosophila* ON and OFF motion detectors enhances real-world velocity estimation. *Nat. Neurosci.* **19**, 706–715 (2016).
53. Pnevmatikakis, E. A. et al. Simultaneous denoising, deconvolution, and demixing of calcium imaging data. *Neuron* **89**, 285–299 (2016).
54. Fişek, M. & Wilson, R. I. Stereotyped connectivity and computations in higher-order olfactory neurons. *Nat. Neurosci.* **17**, 280–288 (2014).
55. Gouwens, N. W. & Wilson, R. I. Signal propagation in *Drosophila* central neurons. *J. Neurosci.* **29**, 6239–6249 (2009).

Author contributions
J.I.-B., H.H.Y., I.E.W. and T.R.C conceived the study. J.I.-B., C.F.R.W., H.H.Y. and Y.E.F. designed and performed the experiments under the supervision of T.R.C. and R.I.W. J.I.-B., K.C.P., H.H.Y., Y.E.F. and I.G.I. generated, maintained and/or validated transgenic fly stocks under the supervision of T.R.C, R.I.W. and G.M. J.I.-B., C.F.R.W., H.H.Y., Y.E.F. and K.C.P. analyzed the data. J.I.-B. and T.R.C. prepared the manuscript with contributions from C.F.R.W., H.H.Y. and Y.E.F.

Competing interests
The authors declare no competing financial interests.

Additional information
Extended data is available for this paper at https://doi.org/10.1038/s41593-020-0668-9.

Supplementary information is available for this paper at https://doi.org/10.1038/s41593-020-0668-9.

Correspondence and requests for materials should be addressed to T.R.C.

Peer review information *Nature Neuroscience* thanks Claude Desplan, Olena Riabinina and the other, anonymous, reviewer(s) for their contribution to the peer review of this work.

Reprints and permissions information is available at www.nature.com/reprints.
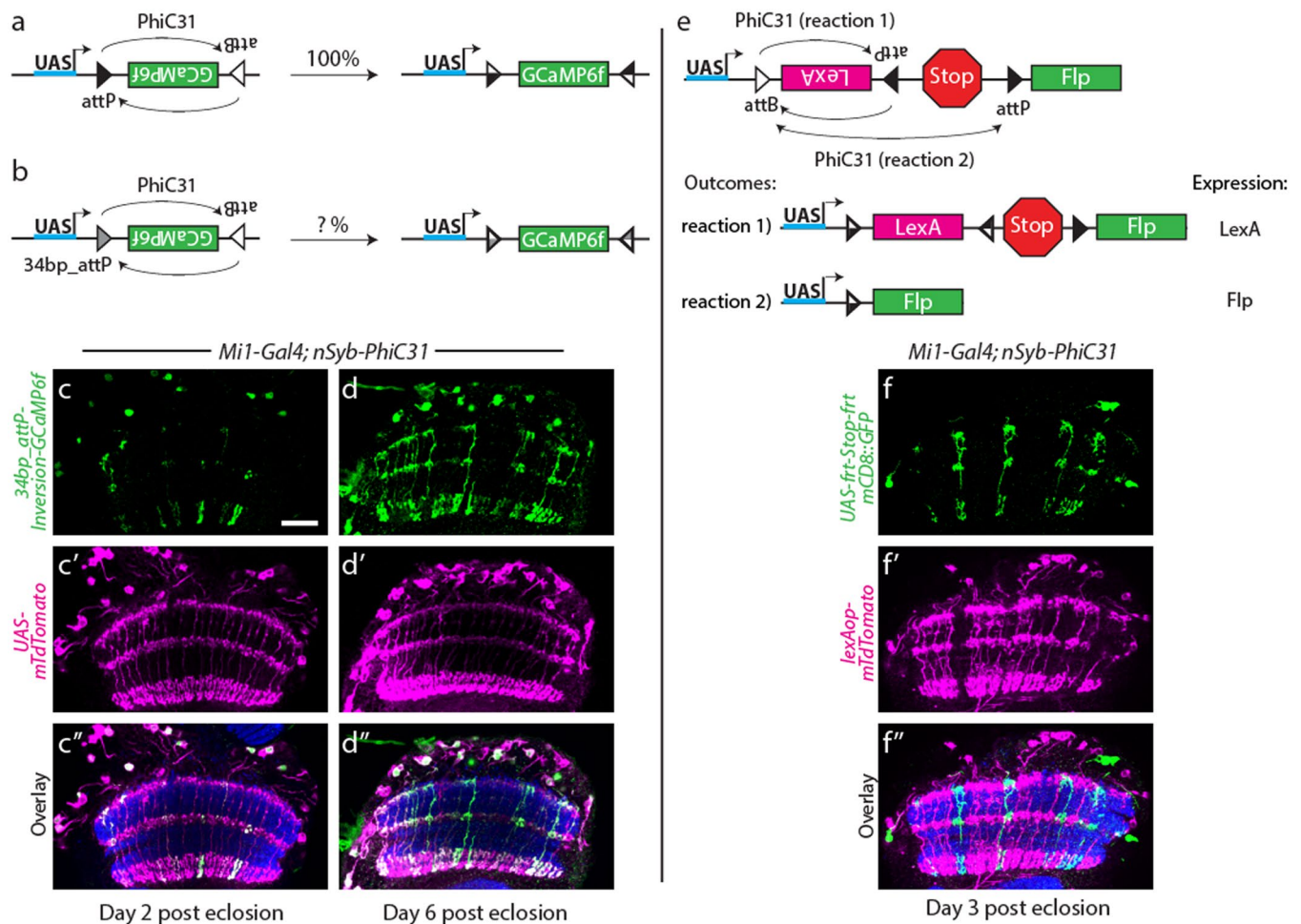
Extended Data Fig. 1 | SPARC development cassettes. a, b, Schematics of PhiC31-dependent *UAS-inversion effector* constructs. (**a**) control construct with canonical *attP* sites and (**b**) truncated *34bp_attP* experimental construct. **c, d″**, *34bp_attP*-Inversion-GCaMP6f expression (green, **c, d**) in Mi1 neurons (magenta, **c′, d′**) counterstained with anti-Bruchpilot (Brp; blue, overlay **c″, d″**). Fewer Mi1 neurons are labeled at day two post eclosion (**c–c″**) than at day six post eclosion (**d–d″**). **e**, Schematic of the LexA-OR-Flp expression construct. PhiC31 recombines one of two competing *attP* target sequences with one *attB* target sequence to enable either LexA or Flp expression. Reaction 1 leads to LexA expression. Reaction 2 leads to Flp expression. **f–f″**, Flp-enabled mCD8::GFP expression (green, **f**) or LexA-driven myr::tdTomato expression in Mi1 neurons (magenta, **f′**) counterstained with anti-Bruchpilot (Brp; blue, overlay **f″**). n = 10 optic lobes per genotype. Scale bar: 10 μm.

a

pHD-3xP3-DsRed-ΔattP
4081bp

Aarl   SphI   NotI   NdeI   Aarl
TCGCTGAAGCAGGTGGAATTCTTGCATGCTAGCGGCCGCGGACATATGCACACCTGCGATCGTAG
EcoRI   NheI   SacII

Multiple Cloning Site L (For Left Homology Arm, HAL)

SapI   BglII   AscI   StuI   PstI   SapI
TATAGAAGAGCGAGCTCACTAGTAAAGATCTCCATGCATAAGGCGCCTAGGCCTTCTGCAGCTCGAGGCTCTTCCGTC
SacI   SpeI   AvrII   XhoI

Multiple Cloning Site R (For Right Homology Arm, HAR)

b

pHD-3xP3-DsRed-ΔattP-
CRISPR-donor
6240bp

NdeI
KpnI
BsiWI

1) Generate homology arms
(Genomic PCR or Synthesis)

2) Clone homology arms into
MCS-L and MCS-R

3) Synthesize SPARC2 Module

4) Clone SPARC2 Module
into restriction enzyme site

5) Replace effector and terminator
by cloning into SalI sites

c

SPARC

20X UAS*   HSP70* Min. Prom.   Stop Sequence**   SalI   Effector (Shown: GCaMP6f)   SalI   SV40 term
attP (D, I, S)   attP   attB

SPARC2

20X UAS*   HSP70* Min. Prom.   Stop Sequence**   HDVR   HDVR   SalI   Effector (Shown: LexA-p65)   SalI   HSP70 term
attP (D, I, S)   attP   attB

*Sequence for these elements was taken directly from pJFRC7
(Addgene #26220 ; Pfeiffer et al. (2010), Genetics, 186: 735-755.)

**Sequence for Stop Sequence was taken directly from pJFRC210
(Addgene #63170 ; Nern et al. (2015), Proc Natl. Acad. Sci., 112:
E2967-E2976.)

Extended Data Fig. 2 | See next page for caption.

Extended Data Fig. 2 | Plasmid maps and molecular cloning methods for SPARC and SPARC2 constructs. a, Map of pHD-3xP3-DsRed-Δ*attP* (a CRISPR-HDR-donor precursor) showing multiple cloning sites for homology arm insertion (right). **b**, Map of pHD-3xP3-DsRed-Δ*attP*-CRISPR-donor (example includes homology arms targeting the *attP40* region of the *Drosophila* genome). **c**, SPARC and SPARC2 cassettes are inserted into pHD-3xP3-DsRed-Δ*attP*-CRISPR-donor via unique KpnI, NdeI, or BsiWI restriction enzyme sites. SalI restriction enzyme sites in the SPARC2 module allow for one-step swapping of the effector and terminator to generate pHD-SPARC2 donor plasmids. Abbreviations: MCS – multiple cloning site; gRNA – guide RNA; HDVR – hepatitis delta virus ribozyme sequence.
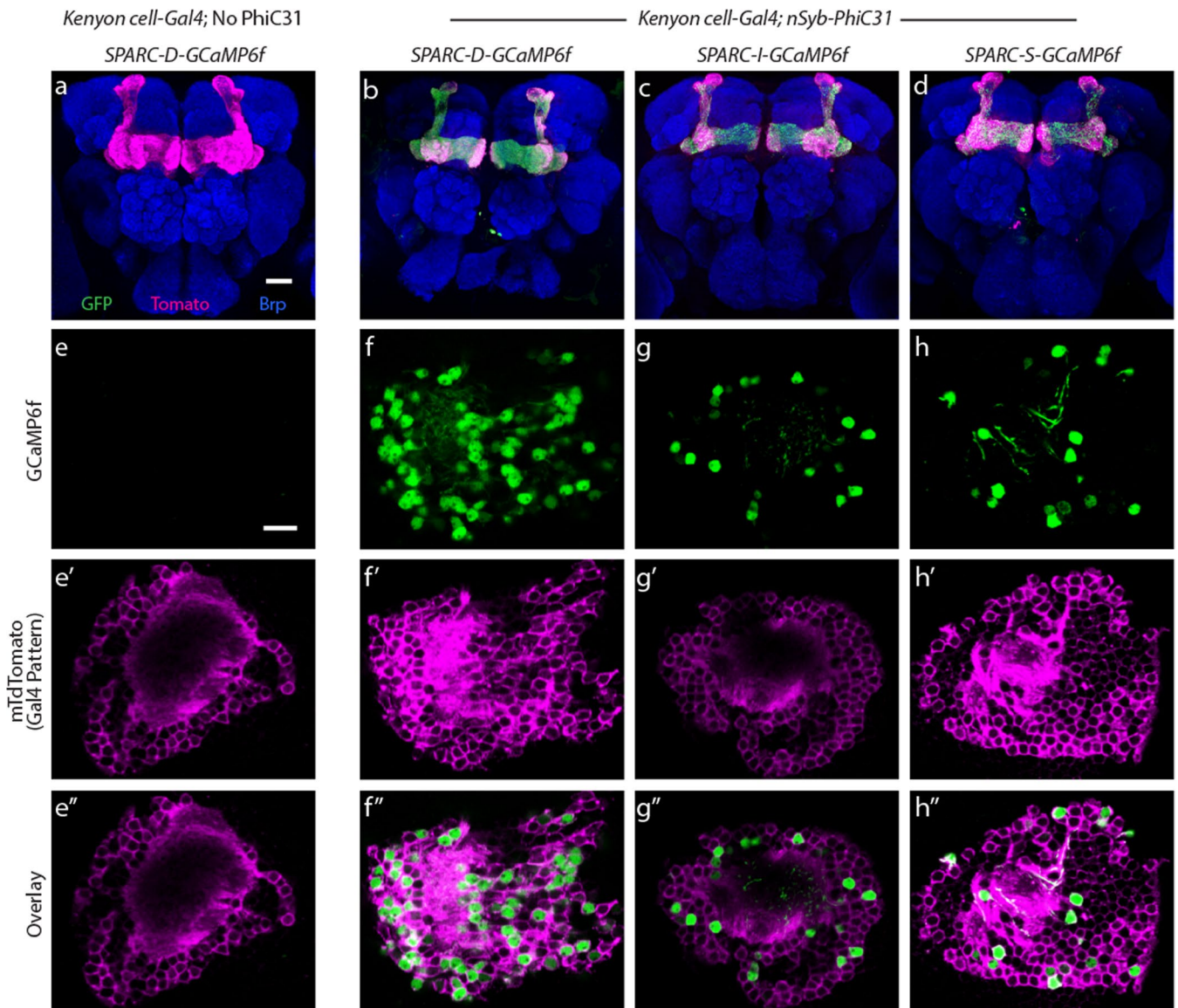
Extended Data Fig. 3 | SPARC-GCaMP6f expression in Kenyon cells. a–d, Anterior view of the *Drosophila* central brain showing GCaMP6f expression (green) in Kenyon cells (magenta) counterstained with anti-Bruchpilot (Brp; blue). **a**, *SPARC-D-GCaMP6f*, no PhiC31. **b**, *SPARC-D-GCaMP6f*. **c**, *SPARC-I-GCaMP6f*. **d**, *SPARC-S-GCaMP6f*. **e–h″**, GCaMP6f expression (green, **e–h**) in Kenyon cell bodies (magenta, **e′–h′**) with overlay (**e″–h″**). **e–e″**, *SPARC-D-GCaMP6f*, no PhiC31. GCaMP6f is not detected in Kenyon Cells in the absence of PhiC31. **f–f″**, *SPARC-D-GCaMP6f*. **g–g″**, *SPARC-I-GCaMP6f*. **h–h″**, *SPARC-S-GCaMP6f*. Scale bars: 30 μm (**a–d**), 10 μm (**e–h″**). n > 10 brains per condition from three independent experiments.

SPARC and SPARC2 user guide

a) Important notes:

1. SPARC and SPARC2 activity requires a minimum of three transgenes: 1) *SPARC-effector*, 2) *promoter-PhiC31*, and 3) *enhancer-GAL4*.

2. *SPARC-effector* or *SPARC2-effector* and *promoter-PhiC31* transgenes <u>MUST</u> be maintained in separate stocks. If both transgenes are present in the same fly, there is a possibility that unanticipated PhiC31 expression in the germline will lead to stable recombination of the *SPARC* or *SPARC2* cassette.

3. For all new *SPARC-effector* combinations, we recommend using SPARC2.

b) Example crossing schemes for SPARC or SPARC2

$$\frac{+}{+} \; ; \; \frac{SPARC2\text{-}Effector}{(near\,\{attP40\})} \; ; \; + \quad X \quad \frac{+}{Y} \; ; \; \frac{promoter^*\text{-}PhiC31}{\{su(Hw)attP5\}} \; ; \; \frac{enhancer\text{-}Gal4}{\{attP2\}} \quad OR$$

$$\frac{+}{+} \; ; \; \frac{SPARC2\text{-}LexA::p65}{(near\,\{attP40\})} \; ; \; \frac{lexAop\text{-}effector}{(variable)} \quad X \quad \frac{+}{Y} \; ; \; \frac{promoter^*\text{-}PhiC31}{\{su(Hw)attP5\}} \; ; \; \frac{enhancer\text{-}GAL4}{\{attP2\}}$$

* Available stocks: *20XUAS-PhiC31, tub-PhiC31,* and *nSyb-PhiC31*

Using split-Gal4 Drivers:

$$\frac{+}{+} \; ; \; \frac{SPARC2\text{-}effector}{(near\,\{attP40\})} \; ; \; + \quad X \quad \frac{promoter^*\text{-}PhiC31\;\{attp18\}}{Y} \; ; \; \frac{enhancer\text{-}GAL4AD^{**}}{\{attP40\}} \; ; \; \frac{enhancer\text{-}GAL4DBD}{\{attP2\}} \quad OR$$

$$\frac{+}{+} \; ; \; \frac{SPARC2\text{-}LexA::p65}{(near\,\{attP40\})} \; ; \; \frac{lexAop\text{-}effector}{\{variable\}} \quad X \quad \frac{promoter^*\text{-}PhiC31\;\{attp18\}}{Y} \; ; \; \frac{enhancer\text{-}GAL4AD}{\{attP40\}} \; ; \; \frac{enhancer\text{-}GAL4DBD}{\{attP2\}}$$

* Available stocks: *20XUAS-PhiC31* and *nSyb-PhiC31*.

** Note: Janelia split-Gal4 drivers use the p65ADZp activating domain[21].

Extended Data Fig. 4 | SPARC and SPARC2 user guide. a, Important notes regarding SPARC and SPARC2 use and stock maintenance. **b**, Example crossing schemes for SPARC or SPARC2 to allow expression of effectors.

nature research

Corresponding author(s):	Thomas R. Clandinin
Last updated by author(s):	2020/05/14

Reporting Summary

Nature Research wishes to improve the reproducibility of the work that we publish. This form provides structure for consistency and transparency in reporting. For further information on Nature Research policies, see Authors & Referees and the Editorial Policy Checklist.

Statistics

For all statistical analyses, confirm that the following items are present in the figure legend, table legend, main text, or Methods section.

n/a	Confirmed	
☐	☒	The exact sample size (*n*) for each experimental group/condition, given as a discrete number and unit of measurement
☐	☒	A statement on whether measurements were taken from distinct samples or whether the same sample was measured repeatedly
☐	☒	The statistical test(s) used AND whether they are one- or two-sided *Only common tests should be described solely by name; describe more complex techniques in the Methods section.*
☒	☐	A description of all covariates tested
☐	☒	A description of any assumptions or corrections, such as tests of normality and adjustment for multiple comparisons
☒	☐	A full description of the statistical parameters including central tendency (e.g. means) or other basic estimates (e.g. regression coefficient) AND variation (e.g. standard deviation) or associated estimates of uncertainty (e.g. confidence intervals)
☐	☒	For null hypothesis testing, the test statistic (e.g. *F*, *t*, *r*) with confidence intervals, effect sizes, degrees of freedom and *P* value noted *Give P values as exact values whenever suitable.*
☒	☐	For Bayesian analysis, information on the choice of priors and Markov chain Monte Carlo settings
☒	☐	For hierarchical and complex designs, identification of the appropriate level for tests and full reporting of outcomes
☒	☐	Estimates of effect sizes (e.g. Cohen's *d*, Pearson's *r*), indicating how they were calculated

Our web collection on statistics for biologists contains articles on many of the points above.

Software and code

Policy information about availability of computer code

Data collection	Leica imaging software
Data analysis	Custom written MATLAB code can be found here: https://github.com/wienecke/SPARC. We used Imaris 9.3, Adobe Photoshop CS6, and FIJI for image analysis. Statistical analyses were performed in MATLAB version r2017b or using socscistatistics.com

For manuscripts utilizing custom algorithms or software that are central to the research but not yet described in published literature, software must be made available to editors/reviewers. We strongly encourage code deposition in a community repository (e.g. GitHub). See the Nature Research guidelines for submitting code & software for further information.

Data

Policy information about availability of data

All manuscripts must include a data availability statement. This statement should provide the following information, where applicable:

- Accession codes, unique identifiers, or web links for publicly available datasets
- A list of figures that have associated raw data
- A description of any restrictions on data availability

All data will be made available upon request from the corresponding authors.

Field-specific reporting

Please select the one below that is the best fit for your research. If you are not sure, read the appropriate sections before making your selection.

☒ Life sciences ☐ Behavioural & social sciences ☐ Ecological, evolutionary & environmental sciences

Life sciences study design

All studies must disclose on these points even when the disclosure is negative.

Sample size	For all experiments, all sample sizes are noted in the text and in the figure legends. Fig. 2-4 at least 5 flies and 10 anatomical regions were analyzed for each genotype. Fig. 5a-e: for each fly/experiment, all ROIs meeting selection criteria described in methods were considered for further analysis; 8 SPARC flies and 8 FlpOut flies were used for analysis. Flies with zero ROIs meeting selection criteria, or with no visually responsive ROIs, were excluded from further analysis (zero SPARC flies, two FlpOut flies). Fig. 6: 5 flies were analyzed for antibody staining, n=4 CsCh+ and n=3 CsCh- neurons were analyzed via electrophysiology. No statistical methods were used to pre-determine sample sizes but our sample sizes are similar to those reported in previous publications (see Methods)
Data exclusions	Flies with zero ROIs meeting selection criteria (methods), or with no visually responsive ROIs, were excluded from further analysis (zero SPARC flies, two FlpOut flies). These exclusion criteria were pre-determined.
Replication	At least two independent experiments were done for each figure panel. Most figure panels show the results from three or more independent experiments and at least 10 individual replicates were observed for each panel (see Figure legends) except for electrophysiological experiments which are technically challenging. All attempts at replication were successful as indicated by statistical tests and dot plots showing individual replicates.
Randomization	All experiments were conducted with independent genotypes that do not require randomization for experimental observation. To the extent possible, genotypes were observed in an interspersed manner between comparisons. For Figure 5, stimulus presentation was randomized.
Blinding	Blind manual cell counting was conducted for Figure 3. We do not believe the other experiments require blinding. Figure 1 is a schematic., Figure 2 involves qualitative comparisons that are validated in statistically in Figure 3. For Figure 4 involves qualitative comparisons that fail to indicate a clear pattern of expression on qualitative inspection. The experiments for Figure 5 validate SPARCs utility as slightly better than previous methods in getting clearer data, but significantly easier technically. Figure 6 shows comparisons within individual animals, blinding is not possible. Extended Data Figures 1 and 3 show data from individual genotypes and are qualitative in nature.

Reporting for specific materials, systems and methods

We require information from authors about some types of materials, experimental systems and methods used in many studies. Here, indicate whether each material, system or method listed is relevant to your study. If you are not sure if a list item applies to your research, read the appropriate section before selecting a response.

Materials & experimental systems

n/a	Involved in the study
☐	☒ Antibodies
☒	☐ Eukaryotic cell lines
☒	☐ Palaeontology
☐	☒ Animals and other organisms
☒	☐ Human research participants
☒	☐ Clinical data

Methods

n/a	Involved in the study
☒	☐ ChIP-seq
☒	☐ Flow cytometry
☒	☐ MRI-based neuroimaging

Antibodies

Antibodies used	Antibodies and concentrations used in this study are as follows: Primary antibodies: anti-GFP (chicken, Abcam ab13970, Cambridge, UK, GB 1:2000, several lots used), anti-Bruchpilot (nc82, mouse, Developmental Studies Hybridoma Bank, Iowa City, IA, USA 1:30, several lots used), anti-DsRed (rabbit, Takara Bio #632496 , Mountain View, CA, USA, 1:700, several lots used). Secondary antibodies: anti-chicken Alexa 488 (1:200, Life Technologies ab150173, Carlsbad, CA, USA, several lots used), anti-rabbit-Cy3 (1:200, A-11008, Thermo Fisher Scientific, Waltham, MA, USA, several lots used), and anti-mouse Alexa 633 (1:200, A-21052, Thermo Fisher Scientific, Waltham, MA, USA , several lots used). Alexa 488-conjugated goat anti-chicken (1:250, A-11039, Thermo Fisher Scientific, Waltham, MA, USA, several lots used), Alexa 568-conjugated goat anti-rabbit (1:250, A-11011, Thermo Fisher Scientific, Waltham, MA, USA, several lots used), and Alexa 633-conjugated goat anti-mouse (1:250, A-21050, Thermo Fisher Scientific, Waltham, MA, USA, several lots used)
Validation	anti-GFP (chicken, Abcam, Cambridge, UK) - validated for IHC in Drosophila, etc...https://www.abcam.com/gfp-antibody-ab13970.html anti-Bruchpilot (nc82, mouse, Developmental Studies Hybridoma Bank, Iowa City, IA) - validated for IF, IHC, WB, in Drosophila, etc...https://dshb.biology.uiowa.edu/nc82 anti-DsRed (rabbit, Takara Bio, Mountain View, CA, USA) - validated for IHC, in n Drosophila, etc...https://www.labome.com/product/Takara-Bio-Clontech/632496.html

Animals and other organisms

Laboratory animals	We used adult female Drosophila Melanogaster in this study at D2-6 Post Eclosion (D4PE on average). The particular genotypes of these animals are described in detail for each experiment in the methods section of this paper.
Wild animals	This study did not involve wild animals.
Field-collected samples	This study did not involve field-collected samples.
Ethics oversight	No ethical approval is required for research with Drosophila Melanogaster

Note that full information on the approval of the study protocol must also be provided in the manuscript.